Cylindrical manifolds in phase space as mediators of chemical reaction dynamics and kinetics. II. Numerical considerations and applications to models with two degrees of freedom

N. De Leon[a)]
Department of Chemistry/Physics/Astronomy, Indiana University Northwest, Gary, Indiana 46408
Manish A. Mehta[b),c)] and Robert Q. Topper[d)]
Department of Chemistry, Yale University, New Haven, Connecticut 06518

(Received 29 March 1990; accepted 26 February 1991)

In Paper I we discussed the existence of cylindrical manifolds embedded in phase space which mediate the dynamics of chemical reactions. A kinetic theory of population decays and decay rate constants was developed which we called "reactive island" (RI) theory. In this paper we discuss the details of the numerical implementation of the theory and then apply it to several molecular models (with two coupled degrees of freedom) representing isomerization between two and three states. Numerical simulations of population decays and asymptotic decay rate constants are compared to the RI theoretical predictions as well as the predictions from the purely random theory (PRT) and transition state theory (TST) of reactions. Of the ten systems studied we find that RI theory is generally in good to excellent agreement with the numerical simulations. Only one system exhibits significant deviation between the RI and numerical results. This deviation is seen to be a result of a strong intraconformer dynamical bottleneck. Finally, we compare the theoretical prediction and the numerical simulation for the average n-map mapping time T_{rxn} and find that the agreement, within numerical error, is exact irrespective of the character of the dynamics (i.e., chaotic or regular).

I. INTRODUCTION

In a previous paper (hereafter referred to as Paper I) we presented a kinetic reaction rate theory based upon the existence of cylindrical manifolds embedded in phase space.[1] These cylindrical manifolds have the property that all pre- and post-reactive motion must pass through their interior. Consequently, these manifolds mediate the dynamics of chemical reactions. A previous paper discussed these manifolds within the context of general Hamiltonian dynamics and chaos.[2] Two earlier papers discussed reactive islands, which are a consequence of the cylindrical manifolds, and their mediation of the reaction dynamics between two conformers.[3,4]

Paper I presented the formal aspects of the theory but did not discuss the technical details necessary to implement the theory or provide explicit kinetic results and data. The objective of this paper is twofold: (1) to describe the details necessary to implement the theory and (2) to apply the theory to several systems and compare the population decays and decay rate constants with those obtained from numerical simulations. Our focus will be primarily on unimolecular isomerization;[5] however, most of the ideas can be extended to bimolecular reactions and unimolecular dissociation as well.[6] In the third paper of this series we will extend the concepts and applications to the unimolecular isomerization of molecular systems with three and more vibrational degrees of freedom (DOF).

Unless otherwise noted, throughout this paper we will assume that the reader is familiar with the contents of Paper I—including both concepts and notation. This paper is arranged in the following manner: In Sec. II we give the numerical procedure for determining symplectic areas of the n-map, reactive islands, overlap areas, etc. Also included in this section is the procedure for determining the RI kinetic mechanism and the details of the numerical simulation. In Sec. III we apply RI theory to several molecular models with two DOF, which serve as general examples of the applicability of RI kinetic theory. Finally in Sec. IV we discuss our results and anticipate the content of Paper III in this series.[7]

II. NUMERICAL CONSIDERATIONS

A. Numerical evaluation of areas

Implementation of RI kinetic theory requires the evaluation of the areas of the reactive islands and the overlap regions within the n-map. One can imagine several ways of accomplishing these tasks. For example, one could explicitly construct the reactive island structure on the n-map and make a direct geometric measurement of this information. This is a crude but nevertheless effective way of obtaining these areas. A more sophisticated way to obtain these areas is to use the action methods of Mackay–Meiss–Percival (MMP).[8–10] MMP have shown that the areas of "turnstiles," which arise from the homoclinic tangle, may be obtained as the difference between the accumulated actions of

[a)] Work performed at Yale University.
[b)] NATO-NSF Postdoctoral Fellow.
[c)] Present Address: Department of Theoretical Physics, University of Oxford, 1 Keble Road, Oxford, OX1 3NP.
[d)] Present address: Department of Chemistry and Supercomputing Institute, University of Minnesota, Minneapolis, MN 55455-0431.

 0021-9606/91/128329-13$03.00

homoclinic orbits. (More will be said about this later.) While the MMP method is accurate, unfortunately it can be difficult to implement since the location of homoclinic orbits is generally a numerically taxing endeavor. Also, this method is at present applicable only to either autonomous Hamiltonian systems with two DOF or nonautonomous Hamiltonian systems with 3/2 DOF and thus not readily extendible to multidimensional systems. However, there is a third, less sophisticated but more practical way to evaluate the overlap areas between reactive islands.

The existence of the phase space cylinders together with area preservation[11] of the n-map dynamics allow one to extract the reactive island structure in an implicit rather than explicit way. We will find that this is the key to making RI theory both practical (i.e., simple to implement) and extendable to multidimensional systems. To see how this may be accomplished we now focus our attention on the reaction dynamics associated with conformational isomerization between two states.

1. Evaluation of $J_\tau(E)$ and n-map areas Σ

The 2-map is defined by the Poincaré mapping surfaces Σ_A^+ and Σ_B^-.[1-4] The initial extension of the cylindrical manifolds $W_A^\pm(E)$ on Σ_A^+ results in the reactive islands II_A^- and II_A^+ (cf. Fig. 1). Depending upon the dynamical system, these reactive islands will or will not overlap one another. The symplectic area of both of these reactive islands is equal to $J_\tau(E)$—the action of the periodic orbit $\tau(E)$,[2]

$$J_\tau(E) = \oint_{\tau(E)} \mathbf{p}\cdot d\mathbf{q}. \tag{1}$$

The evaluation of this integral is a simple task: One evaluates the accumulated action over one cycle of the periodic orbit $\tau(E)$. Equation (1) represents the flux across the potential saddle and has been discussed recently by MacKay.[12]

It is also necessary to evaluate the areas of all mapping surfaces within the n-map. In the 2-map case we need to evaluate the areas of $\Sigma_A^+(E)$ and $\Sigma_B^-(E)$. The area of $\Sigma_A^+(E)$, $\mathrm{Area}(\Sigma_A^+(E))$, is equal to the phase space "volume" of the Hamiltonian $H(q_2,p_2;p_1=0,q_1)$ at energy E. For Hamiltonian systems with two DOF this integral is the same as that given in Eq. (1) except the cycle is over the energetic boundary of $\Sigma_A^+(E)$.

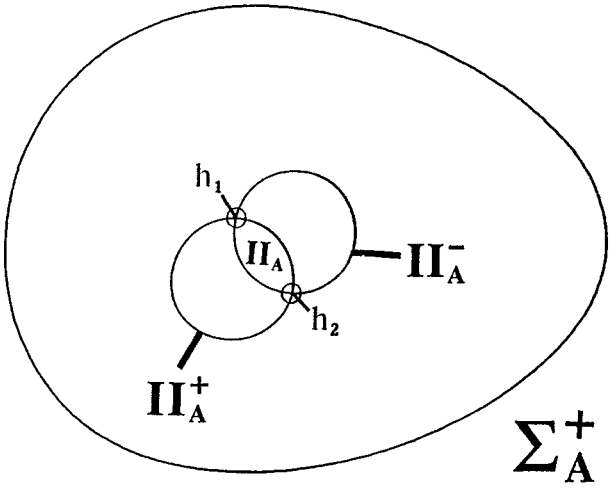

FIG. 1. Schematic drawing of two reactive islands, $\mathrm{II}_A^\pm$, on the mapping plane Σ_A^+. In this case the reactive islands overlap one another forming the region II_A. The points h_1 and h_2 are homoclinic to the periodic orbit τ. The outer closed curve represents the energetic periphery of $\Sigma_A^+(E)$.

2. Evaluation of overlap areas

The evaluation of the overlap areas is relatively more complex than the evaluation of $J_\tau(E)$ or the n-map areas. Nevertheless, it is still a numerically straightforward task. Consider the overlap region labeled II_A in Fig. 1. One way to obtain $\mathrm{Area}(\mathrm{II}_A)$ is to use the methods of MMP. The points of intersection h_1 and h_2 (cf. Fig. 1) between II_A^- and II_A^+ are associated with distinct homoclinic orbits to $\tau(E)$.[11,13] Let F_1 be the accumulated action from $t=-T$ to $t=+T$ of homoclinic orbit h_1,

$$F_1(T) = \left(\int_{-T}^{+T} \mathbf{p}\cdot\frac{d\mathbf{q}}{dt}\,dt\right)_{h_1}. \tag{2}$$

Let F_2 satisfy a similar equation for homoclinic orbit 2, h_2. Using the methods of MMP, one can show that the overlap region II_A is given by[14]

$$\mathrm{Area}(\mathrm{II}_A) = J_\tau(E)\lim_{T\to\infty}\left[1-\frac{|F_1(T)-F_2(T)|}{J_\tau(E)}\right].$$

Successful implementation of Eq. (3) will result in an accurate evaluation of the overlap area II_A. As mentioned above, two major problems arise in the application of the MMP procedure: (1) the homoclinic orbits must be located–a nontrivial numerical task, and (2) the method becomes, for all practical purposes, impossible to apply to systems with more than two coupled DOF (homoclinic orbits are dense for DOF$\geqslant$3). It is therefore apparent that alternate methods are desirable.

The periodic orbit $\tau(E)$ at $q_1=q^\dagger$ encompasses the phase space of a one dimensional "reduced" Hamiltonian $H^{(1)}$ at energy E,

$$H^{(1)}(p_2,q_2) = H(p_2,q_2;p_1=0,q_1=q^\dagger). \tag{3}$$

Motion which begins on $H^{(1)}$ will remain on $H^{(1)}$ for all time. Thus, the phase space encompassed by $H^{(1)}$ is an invariant surface of dimension $N=2$. Suppose that we generate a uniform distribution of N_{TOT} points within the phase space "volume" of $H^{(1)}<E$ (cf. Fig. 2). All such points together with $q_1=q^\dagger$ and p_1 such that $E=H(p_2, q_2,p_1>0,q_1=q^\dagger)$ constitute a uniform ensemble of isoenergetic initial conditions Z [i.e., $Z\in\Sigma^+_{q_1=q^\dagger}(E)$, Eqs. (3) and (4) in Paper I] at the transition state with positive flux. Each of the N_{TOT} points is propagated by Hamilton's equations of motion onto the map Σ_A^+ (cf. Fig. 2). The ensemble of points so generated on Σ_A^+ is uniform since the mapping between the surfaces $T:\Sigma^+_{q_1=q^\dagger}\to\Sigma_A^+$ preserves area. Following this procedure will propagate N_{TOT} points onto the interior of the reactive island II_A^+, Fig. 2. The overlap region II_A is a subset of both of the reactive islands II_A^+ and II_A^-. Conse-

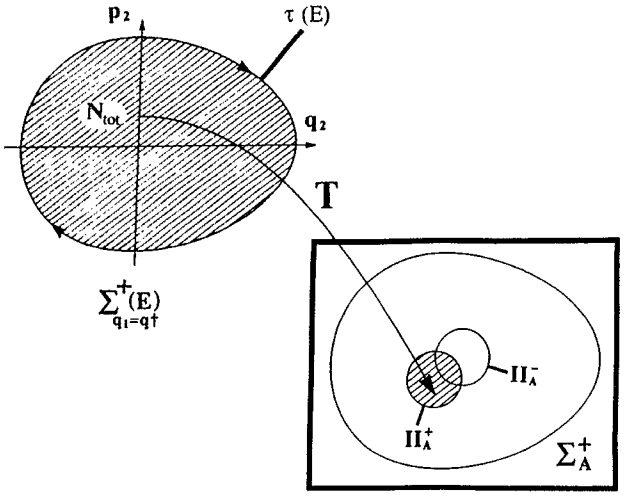

FIG. 2. Schematic drawing of the phase space within the reduced Hamiltonian $H^{(1)}$ phase space (shaded region), i.e., $\Sigma^+_{q_1=q^\dagger}(E)$ (magnified for visualization purposes) mapping onto the Poincare map Σ_A^+ (note that this region must map onto the reactive island II_A^+).

quently all points $Z\in\mathrm{II}_A$ will react onto conformer B upon the 2-map mapping U. We now take all points $Z\in\mathrm{II}_A^+$ and map them by U. After the mapping U a fraction of points $Z\in\mathrm{II}_A^+$ will map back onto Σ_A^+ and a fraction will have mapped onto Σ_B^- (i.e., crossed the barrier), Fig. 3. The number of points that have mapped onto Σ_B^- must be proportional to the area of the overlap region II_A. Let N_1 be the number of points that have not reacted. We will then have

$$\mathrm{Area}(\mathrm{II}_A) = J_\tau(E) \lim_{N_{\mathrm{TOT}}\to\infty}\left(\frac{N_{\mathrm{TOT}}-N_1}{N_{\mathrm{TOT}}}\right),$$

$$\mathrm{Area}(\mathrm{III}_A^+) = J_\tau(E) - \mathrm{Area}(\mathrm{II}_A), \qquad (4)$$

where $\mathrm{III}_A^+ = U(\tilde{\mathrm{II}}_A^+)$. A similar procedure would be used to evaluate $\mathrm{Area}(\mathrm{II}_B)$. Determination of the primary-1 overlap areas enables the calculation of the RI kinetic model which includes primary-1 back reaction [cf. Eq. (18) of Paper I].

Depending upon the specific system under consideration, an RI kinetic model which explicitly includes only primary-1 back reaction may or may not be of adequate accuracy. Suppose that secondary back reaction also contributes significantly to the isomerization dynamics. In such a case it is necessary to include secondary back reaction in the RI kinetic model and thus the area of the overlap region III_A must be determined. After the mapping U, as discussed above, there will be N_1 points uniformly distributed within the reactive island III_A^+, Fig. 3. Each of the N_1 points are once again propagated for another mapping U. A fraction of the N_1 points $Z\in\mathrm{III}_A^+$ will remain in Σ_A^+, Fig. 4. Let N_2 be the remaining number of points within Σ_A^+ after U^2, then

$$\mathrm{Area}(\mathrm{III}_A) = J_\tau(E) \lim_{N_{\mathrm{TOT}}\to\infty}\left(\frac{N_1-N_2}{N_{\mathrm{TOT}}}\right),$$

$$\mathrm{Area}(\mathrm{IV}_A^+) = J_\tau(E) - \mathrm{Area}(\mathrm{II}_A) - \mathrm{Area}(\mathrm{III}_A), \qquad (5)$$

where $\mathrm{IV}_A^+ = U(\tilde{\mathrm{III}}_A^+)$. The RI kinetic mechanism which includes primary-1 plus secondary back reaction from conformer A and only primary back reaction from conformer B is given by Eq. (22) in Paper I.

Clearly, one can continue in this manner to obtain, in succession, the areas of a hierarchy of overlap regions II_A,III_A,IV_A,.... In the next section we discuss the evaluation of area of the map associated with regular motion.

3. Evaluation of Area(R) and Area(T)

The dynamics of Hamiltonian systems is generically characterized by the coexistence of chaotic and regular motion.[11,13] The reaction dynamics, and hence the reaction rate constant, will be influenced by such motion. Consequently, regular motion must be taken into account in the RI kinetic model. If a potential energy barrier is present, then regular motion may be further subdivided into *trapped* and *reactive* regular motion.

Regular motion will consume a finite volume of phase space. From the perspective of maps, regular motion will cover a finite area within the n-map. In the 2-map presently under consideration, the region within Σ_A^+ associated with regular reactive motion is denoted as R_A and with trapped regular motion as T_A (cf. Appendix A in Paper I). Although it is possible that reactive regular motion may be quite complex, in all of the systems we have studied we have found it always to be direct. We will thus develop the ideas below with the assumption that reactive regular motion is direct.[15] In this case it must be true that $R_A \subset \mathrm{II}_A$. The numerical

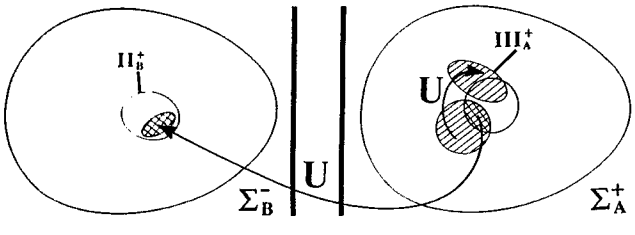

FIG. 3. Schematic drawing of the mapping by U of II_A^+ (cf. Fig. 2). The overlap region II_A maps onto Σ_B^- (and has thus undergone reaction) whereas the region $\tilde{\mathrm{II}}_A^+ = \mathrm{II}_A^+ - \mathrm{II}_A$ maps back onto Σ_A^+ generating the reactive island $\mathrm{III}_A^+ = U(\mathrm{II}_A^+ - \mathrm{II}_A)$.

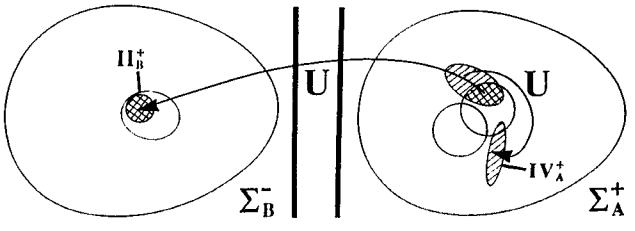

FIG. 4. Same as Fig. 3 except that the mapping U is acting on the reactive island III_A^+ (cf. Fig. 3). The reactive island $\mathrm{IV}_A^+ = U(\mathrm{III}_A^+ - \mathrm{III}_A)$ is generated.

evaluation of Area(R_A) is straightforward: Consider a uniform ensemble of $N_{\rm TOT}$ points $Z \in \Pi_A^+$ (cf. Sec. II A 2). These points are mapped by the 2-map mapping U. After each mapping U, only those points are kept which have reacted. After an infinite number of mappings U the only points left will be those within R_A. Let N_R be the number of points left, then

$$\text{Area}(R_A) = J_r(E) \lim_{N_{\rm TOT}\to\infty} \left(\frac{N_R}{N_{\rm TOT}}\right). \tag{6}$$

Evaluation of the area of T_A is accomplished in a similar manner: Generate an ensemble of $N_{\rm TOT}$ point $Z \in \Sigma_A^+(E)$ and map each of these points by the 2-map mapping U. Each time a point maps onto Σ_B^- it is eliminated from further mapping. After an infinite number of mappings U the only points left in $\Sigma_A^+(E)$ will be those within T_A. If we let N_T be the number of points left in $\Sigma_A^+(E)$, then

$$\text{Area}(T_A) = \text{Area}(\Sigma_A^+(E)) \lim_{N_{\rm TOT}\to\infty} \left(\frac{N_T}{N_{\rm TOT}}\right). \tag{7}$$

The discussion above has focused on conformer A; however it should be obvious that the same methods are applied to conformer B.

Equations (4), (5), and (7) are exact. Equation (6) is exact if all reactive regular motion is direct.[15] However, in practice one is limited in accuracy by computational resources. Both the number of points that must be mapped and the number of mappings each point can undergo is finite. Fortunately, this does not pose a major problem as $N_{\rm TOT}$ and the number of mappings U can be gradually increased until some prespecified convergence is met. In general we have found that the areas need only be obtained to about three significant figures for the population decay and rate constant results of the RI kinetic model to be reasonably accurate.

The only detail in the implementation of RI theory we have not discussed is how to determine the specific RI kinetic mechanism for the system under consideration. These considerations are discussed in detail in the following section.

B. Determination of the RI kinetic mechanism

To construct the RI kinetic mechanism at a total energy E it is necessary to determine (1) the primary-F route to back reaction, (2) the hierarchy of back reaction routes to be explicitly included in the kinetic mechanism.

The method discussed above to determine the areas of the overlap regions II_A,III_A,IV_A,..., etc. will, as a by product, give this information. The procedure as discussed in Sec. II A 2 is carried out along the hierarchy of overlap areas to determine as many of them as desired. The areas so obtained can then be plotted as as a function of the 2-map iteration p (cf. Sec. III B 1). Such a plot will immediately show the primary route to back reaction and will also reveal which routes to back reaction are dominant and thus should be explicitly included in the RI mechanism. For example, if the first peak in this plot is at $p = 1$ then $F = 1$, if the first peak is at $p = 2$ then $F = 2$, etc. The dominant peaks in this hierarchy are the appropriate ones to include in the kinetic model. It is generally obvious which peaks contribute most to the overall flux (cf. Sec. III B 1). Nevertheless, the inclusion of less dominant peaks into the RI model will not perceptibly alter the result. Therefore, a good "rule of thumb" is to include more pathways into the RI model than one would judge to be essential for an accurate result. In this manner one ensures that all dominant back reactive pathways are included in the kinetic model.

Finally, in the following section we briefly discuss initial conditions and the numerical extraction of population decays.

C. Numerical population decays and decay rates

The results of RI theory and numerical simulations are compared by focusing on the n-map population decays and decay rate constants. The numerical simulation is accomplished in the following manner: A uniform distribution of N points on the Poincaré surface $\Sigma_A^+(E)$ at an excess energy ΔE [i.e., a uniform distribution of points $Z \in \Sigma_A^+(E)$] is generated (typically about 5000). Each point so generated represents an initial condition for a trajectory of the full Hamiltonian. Each point is mapped in the n-map K times by the 2-map mapping U. After each mapping U, the number of points that lie on Σ_A^+, $N_A(p)$, is evaluated and is referred to as the population of conformer A. In this manner the normalized population of conformer, $A(p) = N_A(p)/N$ as a function of map iteration p is monitored. The numerical decay rate constant $1/\tau_{\rm rxn}$ is obtained by evaluating the asymptotic slope of the logarithm of $|A(p) - A_{eq}|$ (cf. Sec. III C).

III. APPLICATION OF RI THEORY TO MODEL ISOMERIZATION REACTIONS

A. Molecular isomerization Hamiltonian

In this section we apply the kinetic theory discussed in the above two sections to three distinct two DOF Hamiltonian systems whose dynamics represent molecular conformational isomerization. In all cases the Hamiltonian has the general form

$$H = \frac{1}{2\mu}(p_1^2 + p_2^2) + V(q_1)e^{-z\lambda q_2} + D(1 - e^{-\lambda q_2}) + V_0, \tag{8}$$

where $V(q_1)$ is a fourth- or sixth-order polynomial in q_1 depending upon whether the system has two or three potential minima, cf. Fig. 5. The functional form of $V(q_1)$ will be

$$V(q_1) = V_{DW} = \epsilon q_1^2 (q_1 - a)(q_1 + b),$$
$$V(q_1) = V_{STW} = \epsilon q_1^2 (q_1^2 - a^2)(q_1^2 - b^2). \tag{9}$$

The parameters μ, λ, ϵ, z, D, V_0, a and b used in this investigation are given in Table I. Although the Hamiltonian models described by Eqs. (8) and (9) are not associated with any particular molecule, the details of the dynamics of these models are nevertheless representative of isomerization between two and three conformational states.

RI kinetic theory is applied to these systems for various sets of parameters and total excess energies ΔE above the barrier. The results are then compared to numerical simulations of the population decay rates.

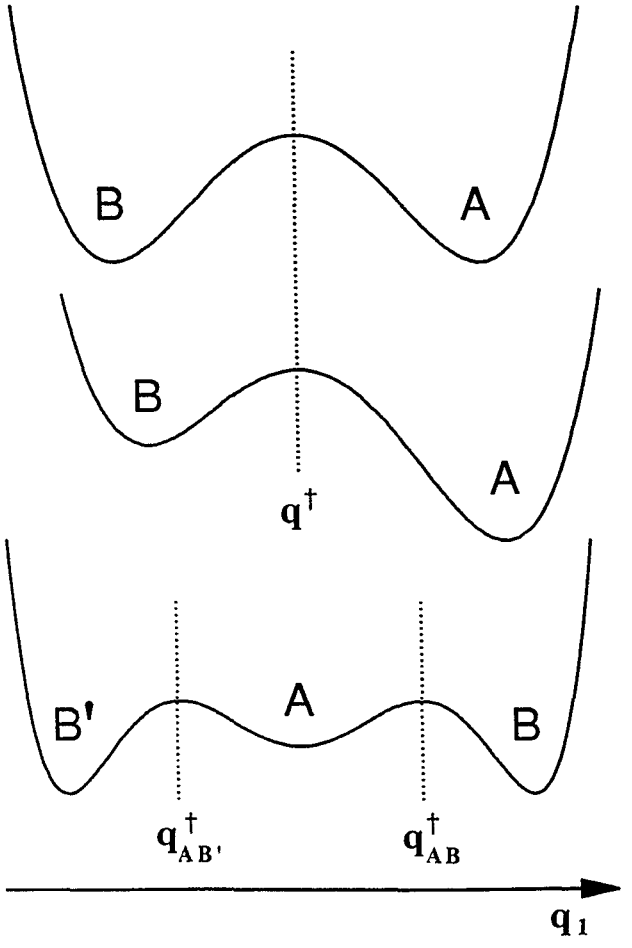

FIG. 5. The potential $V(q_1)$ for the systems studied in this paper. The conformers are labeled as discussed in the text.

B. Symmetric two state systems

We consider two sets of parameters for the symmetric two state Hamiltonian, cf. Table I. Previous studies have shown that there exists very little regular motion for systems 1–3.[2,4] The dynamics for systems 4 and 5 has a mixture of regular and chaotic motion.[16] The reaction dynamics will be examined and modeled by RI theory at several excess energies ΔE. All mapping planes Σ are located about the well minima.

TABLE I. Hamiltonian parameters.[a]

No.	Type[b]	Z	λ	a	b	ΔE
1	SDW	2.3	1.95	1.0	1.0	0.05
2	SDW	2.3	1.95	1.0	1.0	0.20
3	SDW	2.3	1.95	1.0	1.0	1.00
4	SDW	1.0	1.50	1.0	1.0	0.05
5	SDW	1.0	1.50	1.0	1.0	0.50
6	ADW	2.3	1.95	0.9	−1.1	0.05
7	ADW	2.3	1.95	0.9	−1.1	0.50
8[c]	STW	5.0	1.95	0.9	1.0	0.03
9[c]	STW	5.0	1.95	0.9	1.0	0.20
10[c]	STW	5.0	1.95	0.9	1.0	0.45

[a] The following parameters were held constant for systems 1–7 $\mu = 8.0$, $D = 10.0$, $\epsilon = 4.0$, $V_0 = 1.0$. For systems 8–10 $D = 5.0$, $\epsilon = 10.0$, $V_0 = 0$, all other parameters the same.

[b] SDW = symmetric double well, ADW = asymmetric double well, STW = symmetric triple well.

[c] The barrier is at 0.550 078 energy units (e.u.). The well depth of conformers A and B is 0.550 078 and is 0.640 278 e.u., respectively.

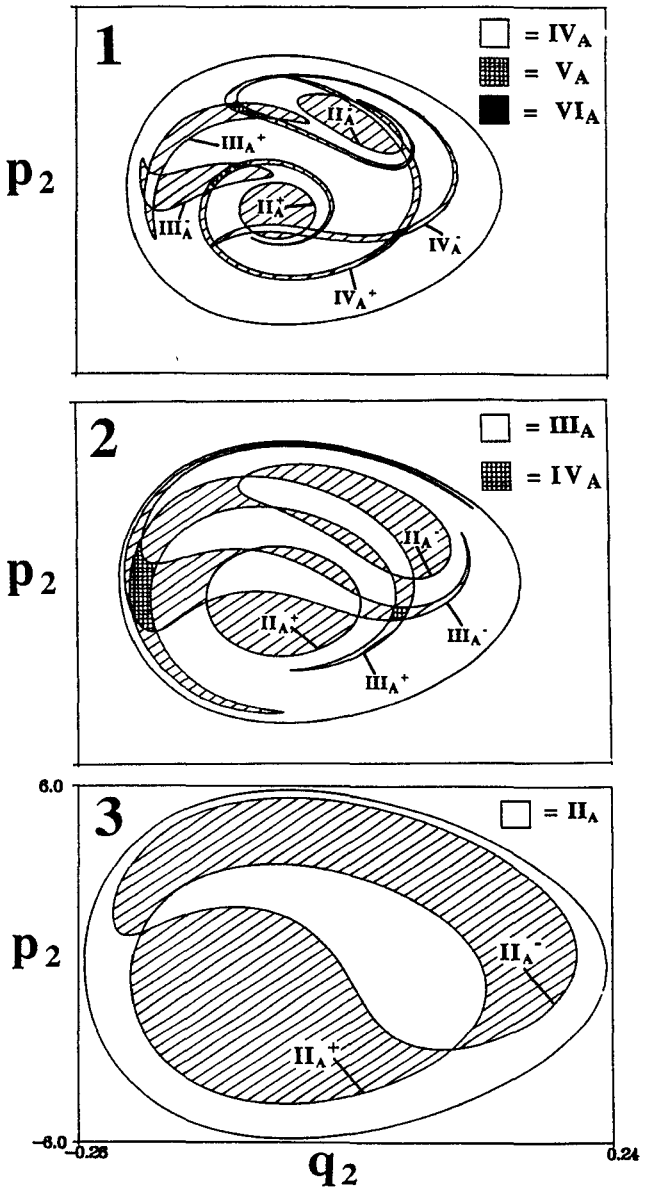

FIG. 6. The low order reactive island structure for systems 1–3. Due to the symmetry in these three systems only the RI structures on Σ_A^+ need be shown. The numbers refer to the system and the legend in the upper right-hand corner identifies the various overlap areas.

1. Systems 1–3: Chaotic motion

In Fig. 6 we show the RI structure on Σ_A^+ for system 1–3. Systems 1, 2, and 3 are at excess energies 0.05, 0.2, and 1.0, i.e., low, intermediate, and high energies, respectively. Due to symmetry, the RI structure on Σ_B^- is the same as that on Σ_A^+. Examination of Fig. 6 reveals that systems 1, 2, and 3 are primary-3, primary-2, and primary-1 systems, respectively.[17] This is further exemplified in Fig. 7 where we plot

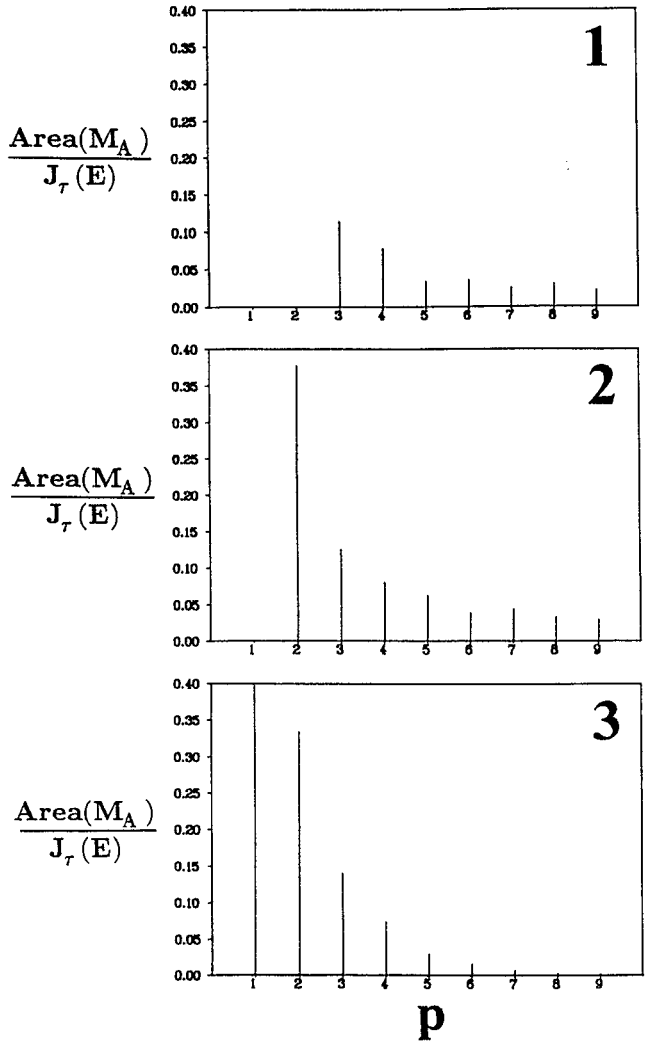

FIG. 7. The "spectrum" of overlap areas for systems 1–3 as a functions of the map iteration p. The reader should note the correspondence between this figure and Fig. 6.

the various overlap areas as a function of the map iteration p, as discussed in Sec. II B.

RI theory allows the explicit inclusion of any number of back reactive pathways into the kinetic model. Ideally, one would include only those pathways that contribute significantly to the overall reaction dynamics. To make the following discussion as simple as possible we will use the following terminology: 1st = primary, 2nd = secondary,..., etc.

For system 1 we explicitly include 1st through 3rd order back reaction in the RI kinetic model. All relevant areas are given in Table II. In Fig. 8 we compare the population decays obtained numerically and from RI theory. The agreement is excellent. In Table III we give the numerical and theoretical n-map decay rate $k_{\rm rxn}$ $(=\tau_{\rm rxn}^{-1}/T_{\rm rxn}^{-1})$, where $T_{\rm rxn}$ is the average n-map mapping time and $\tau_{\rm rxn}^{-1}$ is the microcanonical rate constant for the reaction as given by Eq. (40) in Paper I.[1,18] {In Appendix A we give numerical data for $T_{\rm rxn}$ and compare it with the theoretical value [cf. Eq. (41) of Paper I] for the three state system discussed in Sec. III D.} It appears that RI theory, as well as the purely random theory[1] (PRT) and transition state theory (TST)[19,20] agree well with the numerical result for both the population decay and decay rate. This may appear to support the notion that statistical theories (i.e., TST or RRKM[21,22]) will improve at low excess energies.[23] However, presently we will find that this is not generally the case (cf. Sec. III C). Nevertheless, a close examination of Fig. 8 and Table III shows that RI theory gives a quantitative improvement over PRT.

For system 2 we include 1st through 3rd order back reaction in RI kinetic model. In Fig. 8 we compare the population decays obtained numerically with those obtained from the PRT model and the RI kinetic models. From this figure and Table III it is clear that significant discrepancies exist between the PRT and TST models and the numerical result. However, the RI model continues to be in excellent agreement with the numerical result. Also included in Fig. 8 is the temporal population decay curve (insert). This temporal decay is included as an example of the close correspondence of the populations decays which result from temporal and n-map dynamics. Similar correspondence has been found for all population decays we have studied (see also Sec. II D).

For system 3 we include 1st through 4th order back reaction in the RI kinetic model. The population decay is sufficiently fast that it becomes impossible to extract a numerical rate. Nevertheless, RI, PRT, and TST theory can still be applied. In Fig. 8 and Tables III we compare the numerical and theoretical results. Note from Fig. 8 that RI theory remains in reasonable agreement with the numerical population decay. Any deviations between the RI decay and the numerical decay in Fig. 8 are directly attributable to deviations from the statistical assumption.[24,25] Although RI and TST theory appear to be in close agreement with one another with respect to the decay rate, only RI theory reproduces the population decay in a reasonably accurate manner.

2. Systems 4,5: Regular + chaotic motion

The reaction dynamics of the previous three systems was chaotic over, essentially, the entire phase space at the energies studied. However, chaotic motion generally coexists with regular motion. Systems 4 and 5 (which is the same system as studied in Ref. 14) have a significant amount of regular motion. Parameters for these systems are given in Table I.

Both systems 4 and 5 are primary-1 back reactors. In Tables II and III we give the area and rate data. In both cases the RI kinetic model explicitly included 1st through 3rd order back reaction. In Fig. 9 we compare the numerical population decays with the various theoretical models. Note that RI theory is in quite good agreement with the numerical population decay for both systems. This is also seen to be the case for the rate data in Table III. The slight deviation of RI theory for system 4 can be accounted for by considering intraconformer dynamical bottlenecks. This will be discussed shortly. Also, note the slight oscillations in the population decay in system 5. These oscillations are a direct result of the presence of reactive regular motion (cf. Table II).

TABLE II. Areas.[a,b]

No.	Type[c]	Well	Σ	J_τ	T	R	II	III	IV	V	VI
1	BR	*A*	2.419	0.1020	0.0	0.0	0.0	0.0	0.0116	0.0080	0.0034
2	BR	*A*	2.730	0.4096	0.0	0.0	0.0	0.1540	0.0513	0.0330	0.0260
3	BR	*A*	4.429	2.0920	0.0	0.0	0.829	0.699	0.284	0.154	0.0625
4	BR	*A*	2.779	0.1362	1.11	0.0	0.0220	0.0335	0.0137	0.0072	0.0041
5	BR	*A*	3.987	1.342	0.60	0.05	0.950	0.130	0.035	0.021	0.049
6[d]	BR	*A*	3.278	0.1020	0.0656	0.0	0.0	0.0	0.0	0.014	0.0045
	BR	*B*	1.763	0.1020	0.0599	0.0	0.0	0.041	0.0077	0.0043	0.0023
7	BR	*A*	4.220	1.0320	0.0	0.0	0.029	0.112	0.389	0.189	0.121
	BR	*B*	2.702	1.0320	0.0	0.0	0.391	0.383	0.100	0.044	0.0248
8	TR	*A*	1.723	0.0762	0.005	0.0	0.0	0.0052	0.0043	0.0032	0.0024
	BR	*A*	1.723	0.0762	0.005	0.0	0.0044	0.0066	0.0036	0.0020	0.0018
	BR	*B*	2.126	0.0762	0.17	0.0	0.0022	0.0121	0.0078	0.0019	0.0019
9	TR	*A*	2.249	0.5154	0.0	0.0	0.0949	0.0848	0.0401	0.0197	0.0125
	BR	*A*	2.249	0.5154	0.0	0.0	0.101	0.0697	0.0250	0.0170	0.0134
	BR	*B*	2.691	0.5154	0.0	0.0	0.305	0.0305	0.0075	0.0267	0.0269
10	TR	*A*	3.043	1.156	0.0	0.0	0.487	0.231	0.0747	0.0233	0.0064
	BR	*A*	3.043	1.156	0.0	0.0	0.163	0.120	0.0282	0.0326	0.0103
	BR	*B*	3.543	1.156	0.0	0.0	0.799	0.0550	0.0165	0.0612	0.0482

[a] The areas underlined were used for the RI kinetic models discussed in this paper.
[b] All areas were obtained using 5000–8000 trajectories.
[c] TR and BR signify that the areas are associated with through and back reaction, respectively.
[d] Additional area data for the augmented RI model: Area(α) = 0.088, Area(I^-_{B2}) = 0.984 (as obtained from the 8:3 periodic orbit).

C. Systems 6,7: Two nonequivalent conformers

Systems 1–5, discussed above, correspond to the isomerization dynamics between two equivalent conformers. In this section we extend our application of RI theory to a model of isomerization between two nonequivalent (asymmetric) conformers. The parameters for systems 6 and 7 are given in Table I. Figure 10 compares the numerical and theoretical predictions for the population decay (area data is given in Table II). The numerical and theoretical rate data is given in Table III. All mapping planes Σ within the n-map are located along the various potential well minima.

System 6 is the first system to show significant deviation between the numerical simulation and the standard RI theory as presented in Paper I. In Fig. 10 it appears as though the theoretical and numerical results do not decay to the same equilibrium value. The equilibrium populations can be derived by invoking microscopic reversibility on that fraction of the motion which is chaotic. The RI and PRT theoretical population of conformer A at equilibrium is given by

$$N_A^{eq}(\mathrm{RI}) = N\left[\frac{\mathrm{Area}^2(\Sigma_A^+ - T_A - R_A)}{\mathrm{Area}(\Sigma_A^+)\mathrm{Area}(\Sigma_A^+ + \Sigma_B^- - T_A - T_B - R_A - R_B)} + \frac{\mathrm{Area}(T_A)}{\mathrm{Area}(\Sigma_A^+)} + \begin{cases} \dfrac{\mathrm{Area}(R_A)}{\mathrm{Area}(\Sigma_A^+)}, & \text{if } p = 0,2,4,\ldots; \\ 0, & \text{otherwise} \end{cases}\right], \tag{10a}$$

$$N_A^{eq}(\mathrm{PRT}) = N\left[\frac{\mathrm{Area}(\Sigma_A^+)}{\mathrm{Area}(\Sigma_A^+ + \Sigma_B^-)}\right]. \tag{10b}$$

We will see that the apparent discrepancy between the numerical and theoretical equilibrium populations and rates can be accounted for by internal bottlenecks. Nevertheless, we note from Fig. 10 and Table III that the standard RI theory still gives a better result than either the PRT or TST predictions.

Apparently, the reaction dynamics for this system does not conform well with the statistical approximation (cf. Paper I) in the RI model. What is causing the statistical assumption to fail? The answer can be understood in terms of intramolecular relaxation within a *single* conformer. It is now well appreciated that there can exist dynamical bottlenecks to intramolecular relaxation.[3,24–27,29] These bottlenecks can be associated with the homoclinic and heteroclinic oscillations arising from unstable periodic orbits. These bottlenecks demarcate and control transport within phase

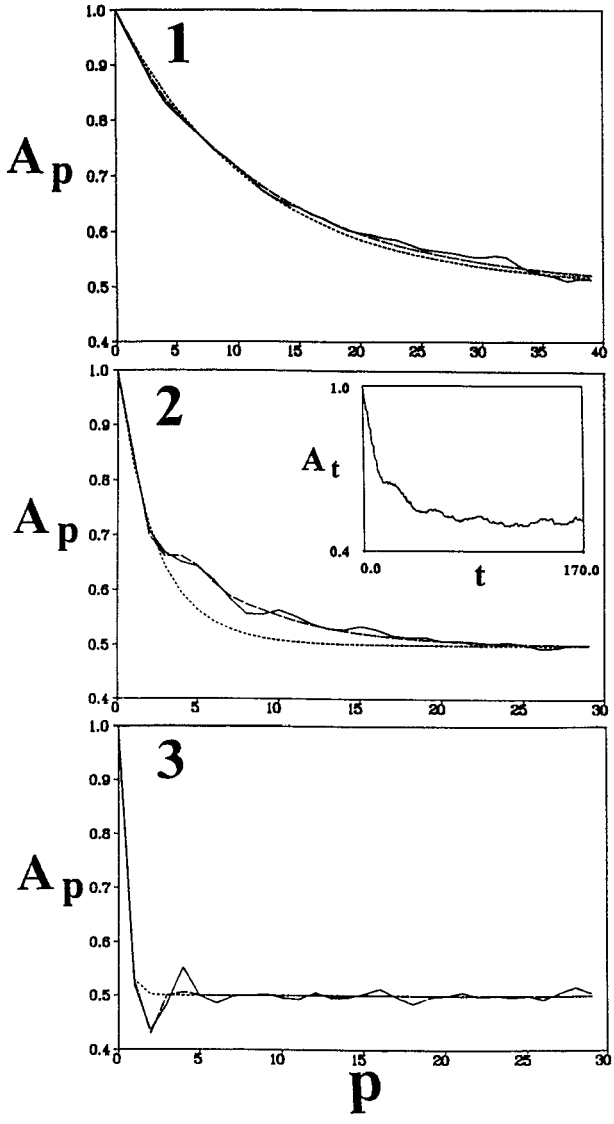

FIG. 8. 2-map population decay curves for systems 1–3 as a function of map iteration p. Numerical simulations are compared with the various theoretical models. Short dash = PRT, long dash = RI theory, and solid = numerical simulation. The inset in Fig. 8(b) is a temporal population decay for system 2. Note the close correspondence between the temporal and map iteration curves. The n-map and temporal numerical simulations were carried out with 5000 trajectories each.

space. Dynamical transport from one region to another is dictated by "turnstiles" which arise from these bottlenecks. Such a dynamical bottleneck exists within conformer B of system 6 and corresponds to a so-called cantorus.[9,26]

In system 6 a central 2:1 resonance exists in conformer B. The appropriate periodic orbit convergents to the cantorus can be identified from the Farey tree[26] and are given by 3:1, 5:2, 8:3, 13:5, 21:8,... . All of these and higher order periodic orbits were found. However, these orbits rapidly become highly unstable and, as a consequence, extremely difficult to connect in the construction of a cantorus. We decided that a rough approximation to the cantorus would be sufficient to account for most of the observed nonstatistical behavior. Thus, we used the 8:3 unstable periodic orbit to

TABLE III. Decay rates $(\tau_{rxn}^{-1}/T_{rxn}^{-1})$.[a]

No.	Numerical	RI theory[b]	PRT[c]	TST[d,e]
1	0.080 (± .002)	0.0797	0.0881	0.0843
2	0.20 (± .01)	0.190	0.414	0.300
3	···	1.08	2.89	0.945
4	0.064 (± .002)	0.066	0.100	0.954
5	0.21 (± .03)	0.211	1.118	0.673
6	0.04 (± .01)	0.0614	0.0932	0.0890
	0.04 (± .01)	0.043[f]	0.0932	0.0890
7	0.27 (± .03)	0.312	0.985	0.626
8	0.048 (± .007)	0.0595	0.083	0.080
9	0.160 (± .02)	0.1652	0.546	0.421
10	0.28 (± .03)	0.299	1.256	0.707

[a] T_{rxn} = characteristic reaction time, and is given by Eq. (41) in Paper I for the two state system, or Eq. (A1) for the three state system.
[b] cf. Eq. (39) in Paper I.
[c] $(\tau_{rxn}^{-1}/T_{rxn}^{-1})_{PRT} = -\ln(1 - P_{A\to B} - P_{B\to A})$, cf. Eq. (12).
[d] $(\tau_{rxn}^{-1}/T_{rxn}^{-1})_{TST} = P_{A\to B} + P_{B\to A}$.
[e] $(\tau_{rxn}^{-1})_{TST} = J_\tau(E)(\rho(E)\chi_A(E)\chi_B(E))^{-1}$, $\rho(E)$ = classical density of states at energy E, $\chi_A(E) = \rho_A(E)\rho^{-1}(E)$ and $\chi_B(E) = \rho_B(E)\rho^{-1}(E)$, i.e., microcanonical equilibrium mole fractions of conformers A and B, respectively (see Appendix C in Paper I).
[f] Rate for augmented RI model.

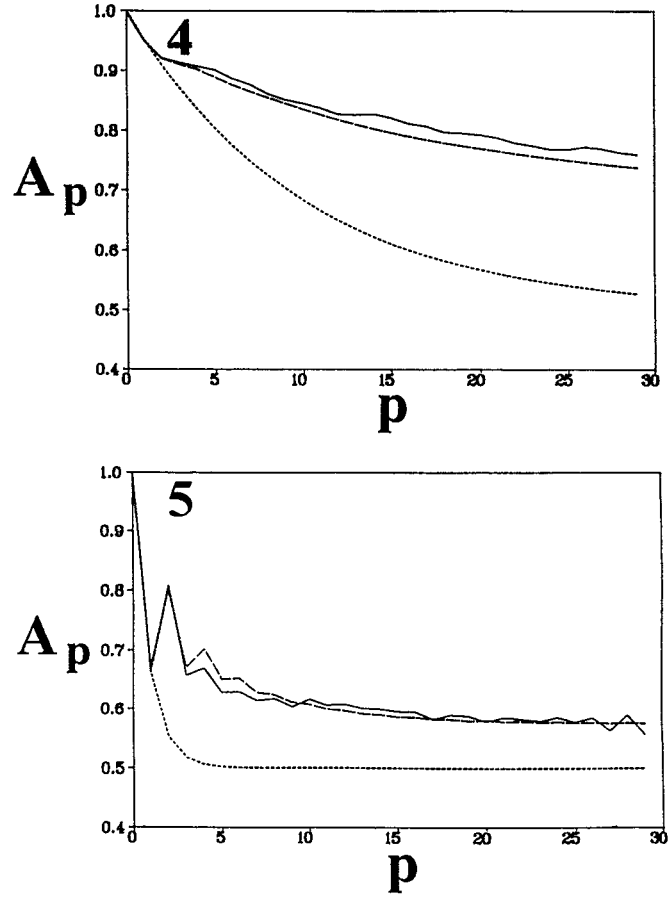

FIG. 9. Same as Fig. 8 except for systems 4,5.

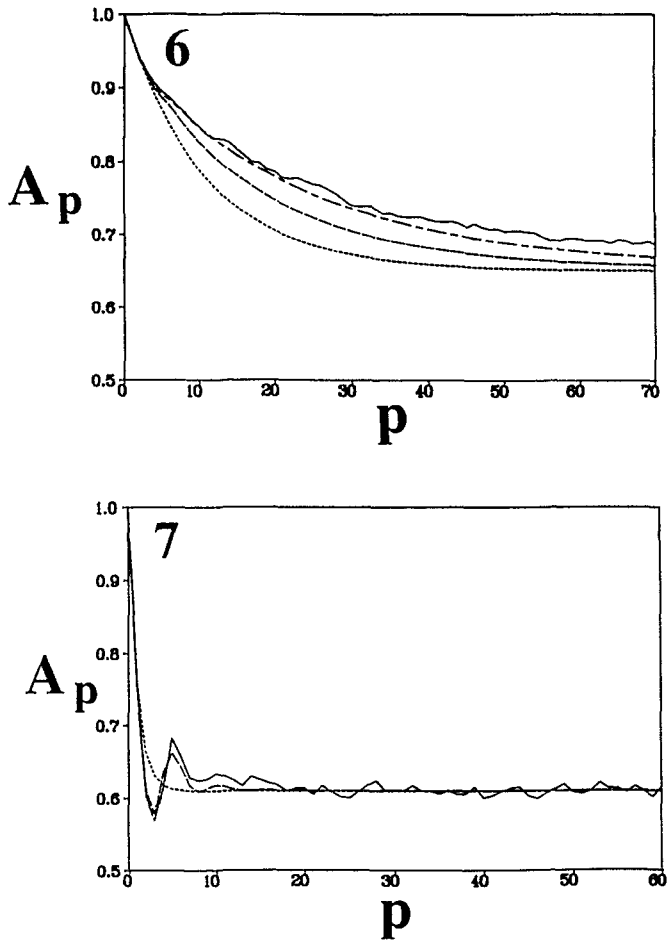

FIG. 10. Same as Fig. 8 except for systems 6 and 7. The curve made up of long and short dashes is the augmented RI model.

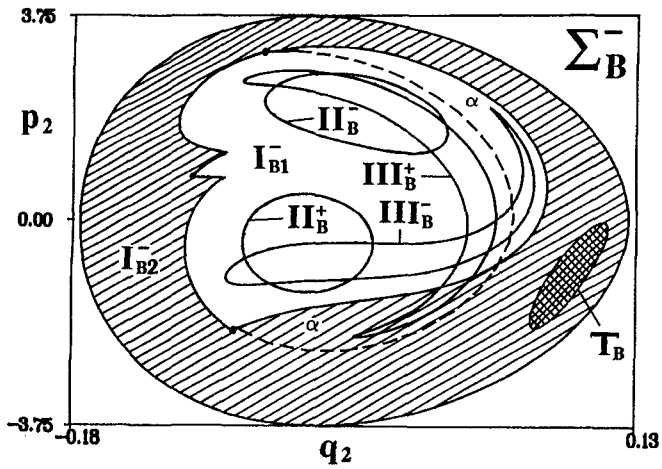

FIG. 11. Low order reactive island structure on Σ_B^- for system 6. Included in this figure is the boundary of the approximate cantorus constructed from the stable and unstable branches of the 8:3 periodic orbit [the initial condition for this periodic orbit on $\Sigma_B^-(E)$ is $q_2 = -0.076\,264\,1$, $p_2 = 3.079\,481\,8$]. The map Σ_B^- is located at the bottom of the well which is at $q_1 = -0.632\,548\,583\,942$. The shaded region is labeled by I_{B1} and the turnstiles are labeled by α.

construct an approximant to the cantorus on $\Sigma_B^-(E)$. The method of doing so has been discussed elsewhere.[26]

In Fig. 11 we plot the approximate cantorus obtained from the 8:3 periodic orbit on Σ_B^-, together with the low order RI structure. The shaded and unshaded regions within I_B^- are separated by the approximate cantorus. Except for a small region associated with trapped regular motion (see Table II), the entire map is associated with chaotic motion. The turnstiles which mediate dynamical transport between the shaded and unshaded regions are labeled α. If we associate this dynamical system with isomerization within a R_1C–CR_2 hindered rotor, then transport across this cantorus can be viewed as energy transfer from a local C–C stretch (q_2) to the isomerization "rotor" mode (q_1) of the molecule.[4]

Transport across the cantorus will take place at a rate determined by the area of the turnstiles. All motion must pass through the reactive island labeled II_B^- prior to reaction onto conformer A. Conversely, all post-reactive motion from conformer A must pass through the reactive island labeled II_B^+. Since II_B^+ lies completely within the unshaded region, post-reactive motion will slowly diffuse into the shaded region—effectively reducing the "trapped" area—at least for the time scale on which Fig. 10 was generated. This explains why it appears as though the numerical result lies above the theoretical equilibrium in Fig. 10. However, it should be noted that if the numerical simulation were propagated for significantly more iterations, that it would eventually decay to the theoretical equilibrium given by Eq. (10).

Standard RI theory (cf. Paper I) can be augmented to take into account the dynamical bottleneck in conformer B. One simply decomposes the region I_B^- into the regions $I_{B_1}^-$ and $I_{B_2}^-$ (cf. Fig. 11) and the RI kinetic equations which include 1st and 2nd order back reaction from conformer A and 1st order back reaction from conformer B would be

$$
\begin{aligned}
&II_A^+(p) = II_B^-(p-1),\\
&III_A^+(p) = II_A^+(p-1),\\
&IV_A^+(p) = III_A^+(p-1),\\
&\tilde{V}_A^+(p) = Q_1^A IV_A^+(p-1),\\
&II_A^-(p) = P_{TR}^A I_A^-(p-1) + P_1^A IV_A^+(p-1)\\
&\qquad + P_2^A \tilde{V}_A^+(p-1),\\
&I_A^-(p) = Q_{TR}^A I_A^-(p-1) + Q_2^A \tilde{V}_A^+(p-1),\\
&II_B^+(p) = II_A^-(p-1),\\
&II_B^-(p) = P_{TR}^B I_{B_1}^-(p-1) + P_1^B II_B^+(p-1),\\
&I_{B_1}^-(p) = (Q_{TR}^B + Q_{12}) I_{B_1}^-(p-1) + P_{21} I_{B_2}^-(p-1)\\
&\qquad + Q_1^B II_B^+(p-1),\\
&I_{B_2}^-(p) = Q_{21} I_{B_2}^-(p-1) + P_{12} I_{B_1}^-(p-1),
\end{aligned}
\tag{11}
$$

where

$$P_{12} = \frac{\text{Area}(\alpha)}{\text{Area}(I_{B_1}^-)}, \quad P_{21} = \frac{\text{Area}(\alpha)}{\text{Area}(I_{B_2}^-)},$$

and $Q = 1 - P$, for all P. The region α is one lobe of the turnstile. The relevant area data is given in Table II. In evaluating the probabilities in Eq. (11) it is important to remember that areas must be subtracted in an appropriate manner to correctly obtain these probabilities (cf. Paper I). The re-

sulting decay curve and rate is shown in Fig. 10 and Table III. The improvement of the augmented RI result over the standard RI result is clearly substantial—although there still appears to be some error. This error is a reflection of the approximate cantorus used and/or the approximate nature of the statistical assumption.

The location of cantori and the determination of the turnstile areas is a relatively simple problem for systems with two DOF systems. However, this is currently a difficult if not impossible problem for systems with three or more DOF[12,29–31] (also see discussion).

The results for system 7 are given in Fig. 10 and Table III. The RI model used consisted of 1st through 4th order back reaction from conformer A and 1st through 3rd order back reaction from conformer B. The area data is given in Table II. RI theory is clearly in excellent agreement with the numerical result whereas PRT and TST are in serious disagreement with it.

D. Systems 8–10: Three conformational states

As our final example of the application of RI theory, we consider the reaction dynamics of a model system which has three potential minima—each of which represents a molecular conformer. The three conformers will be labeled B', A, and B, i.e., Fig. 5. The conformers B and B' are identical and the conformer A lies intermediate between them. The principal distinction between the three and two conformer systems, at least with regard to the kinetic model, is that one must be concerned with *through* (i.e., $B' \rightarrow A \rightarrow B$) reaction as well as back (i.e., $B \rightarrow A \rightarrow B$ or $A \rightarrow B \rightarrow A$) reaction. The three state n-map dynamics, including the RI kinetic model, was discussed in detail in Paper I. It was shown in Paper I that the appropriate RI kinetic mechanism results from a 4-map. In Appendix B we briefly describe the 4-map purely random kinetic model. RI theory will be applied to three systems. All mapping planes Σ within the n-map are located along the various potential well minima (cf. see Sec. IV B in Paper I).

System 8 is at a small excess energy. In Fig. 12 we give the numerical, PRT and RI population decays. In Table II we give the overlap data and in Table III we compare the numerical, RI theory, PRT and TST decay rate constants. From Fig. 12 it is clear that the RI result is a substantial improvement to the PRT (or for that matter the TST) result. The PRT model prediction clearly overestimates the decay rate, cf. Table III. On the other hand there is a perceptible discrepancy between the numerical and RI results. This discrepancy is similar to, though not as pronounced as that seen in system 6 (cf. Fig. 10 and Table III) and can be attributed to intraconformer bottlenecks.[32] Nevertheless, standard RI theory gives a substantially better result than either the PRT or TST theories.

System 9 is at a moderate energy above the barrier. In Fig. 12 we give the various population decays. Tables II and III give the results for the overlaps and decay rates. From Fig. 12 and Table III it is clear that the RI theoretical result is in good to excellent agreement with the numerical result. Both the PRT and TST models are in substantial disagreement with the numerical and RI results.

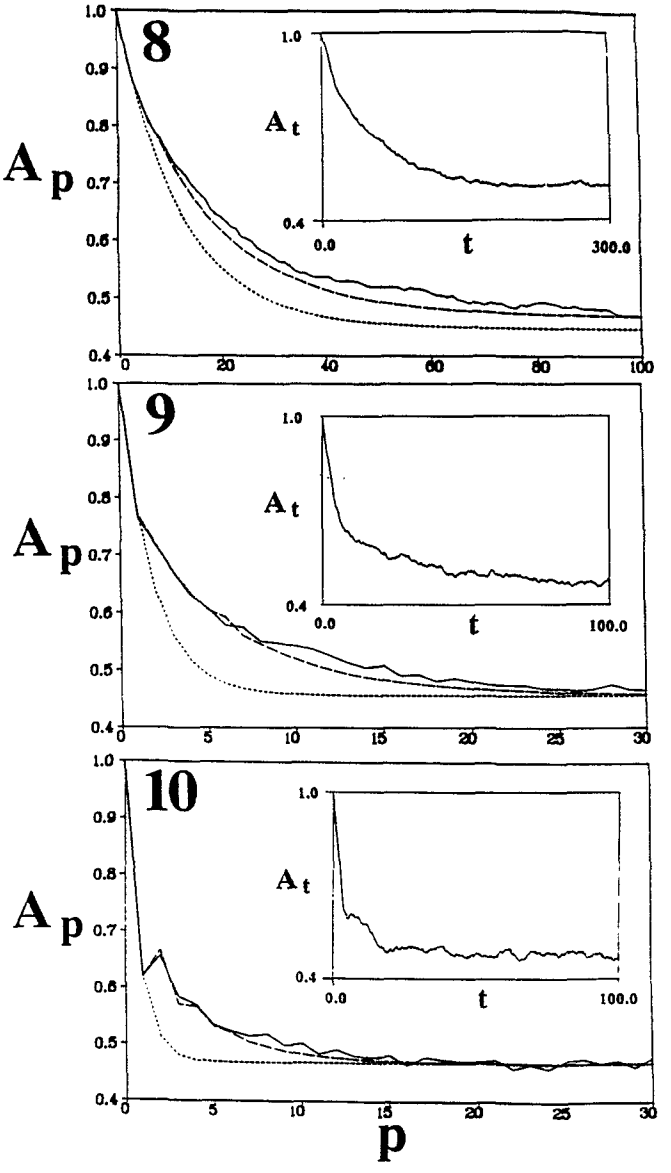

FIG. 12. Same as Fig. 8 except for systems 8–10. Recall that in this case the population decay corresponds to 4-map dynamics. Also included in each decay is the corresponding temporal decay. See text and the appendix for further details.

Finally we consider system 10, which is at a relatively high energy (i.e., almost twice the barrier height). In Fig. 12, Tables II and III we give the population decay, overlap and decay rate data, respectively. Again we see that the RI and numerical results are essentially in exact agreement. Both the PRT and TST models substantially overestimate the decay rate.

IV. DISCUSSION

In Paper I of this series we developed the n-map RI kinetic theory for molecular isomerization between two or more states. In this, the second paper, we discussed the numerical details in the application of the theory and applied it to several systems. The specific steps necessary in the implementation of RI kinetic theory can be succinctly given:

(1) Locate all potential well minima corresponding to different molecular isomers.
(2) Locate all barriers separating potential well minima.
(3) Decide upon appropriate mapping planes Σ to be used in the n-map (cf. Paper I).
(4) Using the methods of Sec. II A, determine the various areas within the n-map mapping planes such as $J_\tau(E)$ [which may necessitate locating the periodic orbit $\tau(E)$], Σ, overlap areas, trapped and reactive regular motion, etc. at a given excess energy ΔE.
(5) Using the information from (4) and the methods in Papers I and II, construct the appropriate RI kinetic mechanism.
(6) Use the information in (4) to determine the various probabilities and construct the RI kinetic equations. The RI kinetic equations can now be solved, given some appropriate boundary conditions (i.e., initial populations), via the methods in Paper I.
(7) The microcanonical decay rate constant may be directly obtained (cf. Paper I) by

$$\tau_{\rm rxn}^{-1}(E) = -T_{\rm rxn}^{-1}(E)\ln(|\lambda_j|). \tag{12}$$

In this paper we have explicitly applied RI theory to several molecular models with two coupled DOF. The results from numerical simulations were compared to the PRT, TST, and RI theoretical models. In all but two cases (systems 6 and 8) it was found that the RI model was in good to excellent agreement with the numerical simulation.

Only in one case (system 6) was the result from the standard RI model in substantial disagreement with the numerical simulation. It was found that this error was a direct consequence of the existence of an intraconformer bottleneck within conformer B. A simple picture of the reaction dynamics emerges: the cylindrical manifolds mediate the dynamical process of reaction and thus may be considered as bottlenecks to transport *between* conformers (i.e., an *interconformer* bottleneck). Manifolds which emerge from unstable motion within a single conformer give rise to bottlenecks to transport *within* a single conformer [i.e., *intraconformer* bottleneck(s)]. Therefore, an accurate description of the global dynamics associated with chemical isomerization must, in general, take into account both intraconformer and interconformer bottlenecks.[33] However, under certain conditions it may only be necessary to consider interconformer bottlenecks (i.e., reactive islands), vis-a-vis systems 1–5,7, 9–10. This simplification is important since the dynamical quantities needed to take into account intraconformer bottlenecks are relatively difficult to obtain. Some insight about when intraconformer bottlenecks must be included in the kinetic model can be gained by noting that if manifolds associated with the intraconformer bottleneck strongly heteroclinically overlap with the cylindrical manifolds, then its effects on the overall reaction dynamics will be relatively minor. The reason for this is simple: a strong heteroclinic overlap indicates that relaxation within a single conformer is heavily mixed with relaxation between conformers. Consequently, under such conditions, phase space will not be subdivided between the two relaxation processes. The standard RI theory should do well under such circumstances. Unfortunately, quantitative ways to predict when we can expect such a strong heteroclinic overlap do not at present exist. It is interesting to note, however, that the work of Davis, Gray, and Rice indicates that these intramolecular bottlenecks can be significant even at high energies.[24,25] As discussed in Sec. II C, intraconformer bottlenecks can be included in an "augmented" RI kinetic model. Unfortunately, the numerical procedures to determine areas of turnstiles associated with intraconformal bottlenecks cannot presently be extended, in a computationally feasible way, to systems with more than two coupled DOF. This is known to be a difficult problem for which there does not currently exist a practical solution.[30,31] The extension, as well as the direct application of RI theory to molecular models with more than two degrees of freedom is the subject of the third paper in this series.

The reader familiar with the numerical techniques used in this papers' implementation of RI kinetic theory will realize that the computer time required by the numerical calculations was not insignificant. This may lead one to question what advantages the theoretical model offers over direct numerical simulation of population decays. Our primary concern in this implementation of RI theory is not motivated by the construction of efficient computational algorithms. Rather, our motivation is to develop a reaction rate theory which predicts populations and rates based upon fundamental properties of Hamiltonian systems such as actions of orbits, turnstile areas, reactive island areas, etc.—thus yielding insight about the microscopic processes within a chemical reaction. Also, it is expected that in the future researchers will develop analytical methods to calculate the above properties.[8–10,34,35] However, these comments should not be taken to construe that the numerical calculations in this paper were prohibitive. Although we did not attempt to optimize our code or conduct systematic studies, we found the amount of computer time necessary to carry out the RI calculations was never more than that of the temporal simulations and often much less.

Finally, it is interesting to note that RI theory has some ideas in common with the work on "direct" and "strong collision" dynamics by Hamilton and Brumer.[36] One can view the kinetic theory as basically a demarcation of the dynamics into strong and direct collision components, where the dynamics is statistical and nonstatistical, respectively. Hamilton and Brumer seek to identify direct vs strong collision dynamics by focusing on the divergence between nearby trajectories as they evolve in time. On the other hand such motion would, according to RI theory, be distinguished according to its position in the kinetic mechanism hierarchy. While these two approaches are quite distinct, they nevertheless share a common goal and their unification may prove to be instructive and beneficial.

APPENDIX A

In Paper I we derived the theoretical expression for the characteristic reaction time $T_{\rm rxn}$ for the case of two conformational states. As discussed in that paper, $T_{\rm rxn}$ is basically the average mapping time between the n mapping planes which, together, define the n-map (i.e., the average n-map

mapping time). In this appendix we compare the numerical and theoretical evaluation of $T_{\rm rxn}$.

The system we will consider in this appendix is the three conformational state system discussed in Sec. III D. Equation (41) for $T_{\rm rxn}$ in Paper I was for a 2-map, whereas the three state system under consideration requires a 4-map.[1] It is straightforward to extend the methods in Appendix B of Paper I to derive the appropriate formula for $T_{\rm rxn}$. The result for the 4-map is

$$T_{\rm rxn}(E) = \frac{\rho(E)}{\text{Area}(\Sigma_B^+(E) + \Sigma_{B'}^-(E) + \Sigma_A^+(E) + \Sigma_A^-(E))}, \tag{A1}$$

where all mapping planes Σ are located along the bottom of the potential wells (see Sec. III D). The full density of states $\rho(E)$ [$= \text{Tr}(\delta(H-E))$] was evaluated via Monte Carlo integration. The results over several energies are given in Table IV. The numerical evaluation of $T_{\rm rxn}$ was accomplished in the following way. N points were uniformly distributed on the 4-map. The number of points on each map within the 4-map was directly proportional to the area of that map, thus ensuring that the distribution of points among the four mapping planes had a uniform density. Each of the N points within the 4-map was propagated for a single 4-map mapping U. The time necessary for each point to undergo the mapping U was accurately evaluated using the Henon algorithm.[37] The average time over the N points was then obtained. These numerical results are compared with the theoretical results as given by Eq. (A1) in Table IV. From this table it is evident that the theoretical and numerical results are in excellent agreement. Two additional points should be made. First, the three state system exhibits regular as well as chaotic motion. Consequently, the agreement between the theoretical and numerical results in Table IV is a demonstration that the calculation of $T_{\rm rxn}$ does not depend upon the characteristics of the dynamics—as long as the mapping planes are attractive.[1,38] Second, $T_{\rm rxn}$ initially increases and then decreases with energy. This interesting behavior of $T_{\rm rxn}$ can be be understood in the following way. Typically, the time it takes a point to undergo a mapping U between adjacent conformers (interconformal mapping) is larger than the time it takes a point to undergo a mapping U within a single conformer (intraconformal mapping). Just slightly above the barrier practically all mappings within the n-map will be intraconformal resulting in a low value for $T_{\rm rxn}$. At higher energies a significant fraction of the mapping is interconformal, resulting in an increase in $T_{\rm rxn}$. At still higher energies the time it takes for interconformal mappings decreases because the walls of the potential go as the sixth power of the reaction coordinate q_1, resulting in a decrease of $T_{\rm rxn}$.

TABLE IV. Theoretical and numerical calculation of $T_{\rm rxn}$.

Energy	$\rho(E)$ [a]	Area(Σ_A) [b]	Area(Σ_B) [c]	$T_{\rm rxn}$ [d]	$T_{\rm rxn}$ [e]	σ [f]
0.58	24.60	1.7230	2.1261	3.20	3.2	1.50
0.69	30.51	2.0623	2.4900	3.35	3.3	1.47
0.75	33.25	2.2492	2.6906	3.37	3.4	1.46
0.875	38.56	2.6429	3.1133	3.35	3.4	1.44
1.00	43.40	3.0426	3.5426	3.30	3.3	1.40
1.25	52.66	3.8611	4.4239	3.18	3.2	1.41
1.5	61.53	4.7074	5.3366	3.06	3.1	1.39

[a] 12×10^6 points were used for the Monte Carlo calculation of $\rho(E)$.
[b] $\text{Area}(\Sigma_A^+(E)) = \text{Area}(\Sigma_A^-(E))$.
[c] $\text{Area}(\Sigma_B^+(E)) = \text{Area}(\Sigma_{B'}^-(E))$.
[d] Theoretical value [cf. Eq. (A1)].
[e] Numerical value using a sampling of 5000 points on the 4-map; the error throughout is roughly 0.05.
[f] Standard deviation in the n-map mapping time distribution at energy E.

APPENDIX B

In this appendix we describe the purely random kinetic model for the three conformer system in Sec. III D and briefly state the principal results. A close examination of this appendix together with Sec. IV C of Paper I should give the reader a general idea of the construction of the purely random kinetic model for any n-map.

The four mapping planes are given in Eq. (28) of Paper I. The dynamical mapping between these four planes according to the purely random model is given by

$$\begin{array}{ccccc} & & \Sigma_A^+ & & \\ P_B \nearrow & & \Uparrow & & \searrow P_A \\ \Sigma_{B'}^- & Q_A & & Q_A & \Sigma_B^+ \\ \nwarrow P_A & & \Downarrow & & \swarrow P_B \\ & & \Sigma_A^- & & \end{array} \tag{B1}$$

where

$$P_A = \frac{J_\tau(E)}{\text{Area}(\Sigma_A^+(E))}, \qquad P_B = \frac{J_\tau(E)}{\text{Area}(\Sigma_B^+(E))}. \tag{B2}$$

Letting $\Sigma_B^+(p)$ denote the population of conformer B at the pth map iteration, etc., the kinetic equations are

$$\begin{aligned} \Sigma_B^+(p) &= Q_B\Sigma_B^+(p-1) + P_A\Sigma_A^+(p-1), \\ \Sigma_A^+(p) &= P_B\Sigma_{B'}^-(p-1) + Q_A\Sigma_A^-(p-1), \\ \Sigma_A^-(p) &= P_B\Sigma_B^+(p-1) + Q_A\Sigma_A^+(p-1), \\ \Sigma_{B'}^-(p) &= Q_B\Sigma_{B'}^-(p-1) + P_A\Sigma_A^-(p-1). \end{aligned} \tag{B3}$$

These equations may be easily solved to yield the eigenvalues $\lambda_1,\ldots,\lambda_4$. These eigenvalues are

$$\begin{aligned} &\lambda_1 = 1, \quad \lambda_2 = 1 - P_A - P_B, \\ &\lambda_3 = \tfrac{1}{2}\left[P_A - P_B + \sqrt{(P_A-P_B)^2 + 4(1-P_A-P_B)}\,\right], \\ &\lambda_4 = \tfrac{1}{2}\left[P_A - P_B - \sqrt{(P_A-P_B)^2 + 4(1-P_A-P_B)}\,\right]. \end{aligned} \tag{B4}$$

The population in conformer A at map iteration p, $A(p)$, is given by Eq. (35) in Paper I. The expansion coefficients a_3 and a_4 associated with the eigenvalues λ_3 and λ_4 are zero so that the population decay is governed by a single exponential with a rate determined by the eigenvalue λ_2.

[1] N. De Leon, Manish A. Mehta, and R. Q. Topper, J. Chem. Phys. **94**, 8310 (1991).
[2] A. Ozorio de Almeida, N. De Leon, Manish A. Mehta, and C. Clay Marston, Physica D **46**, 265 (1990).
[3] C. Clay Marston and N. De Leon, J. Chem. Phys. **91**, 3392 (1989).
[4] N. De Leon and C. Clay Marston, J. Chem. Phys. **91**, 3405 (1989).
[5] W. Forst, *Theory of Unimolecular Reactions* (Academic, New York, 1973).
[6] E. E. Nikitin, *Theory of Elementary Atomic and Molecular Processes* (Clarendon, Oxford, 1974).
[7] N. De Leon, Manish A. Mehta, and R. Q. Topper (in preparation).
[8] R. S. MacKay, J. D. Meiss, and I. C. Percival, Physica D **13**, 55 (1984).
[9] R. S. MacKay, J. D. Meiss, and I. C. Percival, Physica D. **27**, 1 (1987).
[10] R. S. MacKay and J. D. Meiss, J. Phys. A **19**, L225 (1986).
[11] A. J. Lichtenberg and M. A. Lieberman, *Regular and Stochastic Motion* (Springer-Verlag, New York, 1983).
[12] R. S. MacKay, Phys. Lett. A **145**, 425 (1990).
[13] A. M. Ozorio de Almeida, *Hamiltonian Systems: Chaos and Quantization* (Cambridge University, Cambridge, England, 1988).
[14] Direct application of the difference formulas of MMP will yield the area of $\mathrm{II}_A^- - \mathrm{II}_A$, i.e.,

$$\mathrm{Area}(\mathrm{II}_A^- - \mathrm{II}_A) = \lim_{T\to\infty} (|F_1(T) - F_2(T)|).$$

However, we want the overlap area II_A, which is now simple to obtain since we we know the total area of the reactive island $J_{\tau(E)}$, i.e., Eq. (3).
[15] We do not exclude the possibility that reactive regular motion may not be direct (i.e., oscillate more than once within a conformer before recrossing the dividing surface). The extension of the ideas in Sec. II A 3 can be extended to these more complicated cases in a straightforward manner.
[16] S. K. Gray and S. A. Rice, J. Chem. Phys. **86**, 2020 (1987).
[17] The reader is encouraged to follow the reactive island sequences in Fig. 6 and see that this result must indeed be the case.
[18] The microcanonical rate constants $k_{A\to B}(E)$ and $k_{B\to A}(E)$ are related to $\tau_{\mathrm{rxn}}^{-1}(E)$ by $k_{A\to B}(E) = \chi_A(E)\tau_{\mathrm{rxn}}^{-1}(E)$ and $k_{B\to A}(E) = \chi_B(E)\tau_{\mathrm{rxn}}^{-1}(E)$, where χ_A and χ_B are the microcanonical equilibrium mole fractions of conformers A and B, $\chi_A(E) = \rho_A(E)/\rho(E)$, $\rho_A(E)$ and $\rho(E)$ are the classical density of states of conformer A and the full system, respectively.
[19] P. Pechukas, *Dynamics of Molecular Collisions, Part B*, edited by W. H. Miller (Plenum, New York, 1976).
[20] D. G. Truhlar, W. L. Hase, and J. T. Hynes, J. Phys. Chem. **87**, 2664 (1983).
[21] R. A. Marcus, J. Chem. Phys. **20**, 359 (1952).
[22] W. L. Hase, *Dynamics of Molecular Collisions, Part B*, edited by W. H. Miller (Plenum, New York, 1976).
[23] E. Pollak and P. Pechukas, J. Chem. Phys. **69**, 1218 (1978).
[24] M. J. Davis and S. K. Gray, J. Chem. Phys. **84**, 5389 (1986).
[25] S. K. Gray, S. A. Rice, and M. J. Davis, J. Phys. Chem. **90**, 3470 (1986).
[26] M. J. Davis, J. Chem. Phys. **83**, 1016 (1985).
[27] C. C. Martens, M. J. Davis, and G. S. Ezra, Chem. Phys. Lett. **142**, 519 (1987).
[28] S. H. Tersigni, P. Gaspard, and S. A. Rice, J. Chem. Phys. **92**, 1775 (1989).
[29] It is important to stress that this difficulty does not extend to the overlap areas within the RI, or other quantities needed by the standard RI theory.
[30] M. Toller, G. Jacucci, G. DeLorenzi, and C. P. Flynn, Phys. Rev. B **32**, 2082 (1985).
[31] R. E. Gillilan and W. P. Reinhardt, Chem. Phys. Lett. **156**, 478 (1989).
[32] Regular trapped motion is present in conformer A. Its inclusion in the RI kinetic model does not improve it perceptibly.
[33] It should be stressed that this conclusion is not unanticipated. Gray, Rice, and Davis have considered intermolecular as well as intramolecular dynamical bottlenecks in the reaction dynamics of $HeI_2 \to He + I_2$ at very high excess energies. Gray and Rice have considered interconformational bottlenecks (Ref. 18). However, their model is not based upon reactive islands arising from the periodic orbit τ.
[34] A. M. Ozorio de Almeida, Nonlinearity **2**, 519 (1989).
[35] R. S. MacKay and J. D. Meiss, *Hamiltonian Dynaical Systems* (Adam Hilgar, Bristol, 1987).
[36] I. Hamilton and P. Brummer, J. Chem. Phys. **82**, 1937 (1985).
[37] M. Henon, Physica D **5**, 412 (1982).
[38] S. Wiggins, *Global Bifurcations and Chaos* (Springer-Verlag, New York, 1988).